Published in final edited form as:
Inorg Chem. 2007 August 6; 46(16): 6767–6774. doi:10.1021/ic700395j.

Kinetics and Mechanism of Oxidation Reactions of Porphyrin-Iron(IV)-Oxo Intermediates

Zhengzheng Pan and **Martin Newcomb***
Department of Chemistry, University of Illinois at Chicago, 845 W. Taylor Street, Chicago, Illinois 60607

Abstract

The kinetics of reactions of three porphyrin-iron(IV)-oxo derivatives with alkenes and benzylic alcohols were measured. The iron-oxo systems studied were 5,10,15,20-*tetrakis*(2,6-dichlorophenyl)porphyrin-iron(IV)-oxo (**2a**), 5,10,15,20-*tetrakis*(2,6-difluorophenyl)porphyrin-iron(IV)-oxo (**2b**), and 5,10,15,20-*tetrakis*(pentafluorophenyl)porphyrin-iron(IV)-oxo (**2c**). Species **2** were stable for hours at room temperature as dilute solutions in acetonitrile and reacted hundreds to thousands of times faster in the presence of high concentrations of substrates. Typical second-order rate constants determined from pseudo-first-order kinetic studies are $1–2 \times 10^{-2}$ M^{-1} s^{-1} for reactions with styrene and 3×10^{-2} M^{-1} s^{-1} for reactions with benzyl alcohol. The reactivity order for the iron-oxo species was **2a** > **2b** > **2c**, which is inverted from that expected on the basis of the electron demand of the porphyrin macrocycles, and the oxidation reaction was suppressed when excess porphyrin-iron(III) complex was added to reaction mixtures. These observations indicate that the reactions involve disproportionation of the iron(IV)-oxo species **2** to give an iron(III) species and a more highly oxidized iron species, presumed to be iron(IV)-oxo porphyrin radical cation, that is the true oxidant in the reactions. Analyses of the kinetics of oxidations of a series of *para*-substituted benzylic alcohols with Hammett σ^+ substituent constants and with a dual parameter method developed by Jiang (Jiang, X. K. *Acc. Chem. Res.* **1997**, *30*, 283) indicated that considerable positive charge developed on the benzylic carbons in the oxidation reactions, as expected for electrophilic oxidants, and also that substantial radical character developed on the benzyl carbon in the transition states.

High-valent porphyrin-iron-oxo derivatives are thought to be the active oxidants in heme-containing peroxidase, catalase, and cytochrome P450 enzymes,[1–4] and porphyrin-iron complexes are among the better known laboratory catalysts.[5,6] In catalytic processes, porphyrin-iron(III) species are oxidized by sacrificial oxidants such as *m*-chloroperoxybenzoic acid (MCPBA) or iodosobenzene, PhIO. Depending on the identity of the porphyrin, solvents and reaction conditions, either porphyrin-iron(IV)-oxo or iron(IV)-oxo porphyrin radical cations can be detected in these reactions, and both are generally thought to be active oxidants. In biological contexts, iron(IV)-oxo porphyrin radical cations are commonly referred to as Compounds I. Compound I species are detected in peroxidase enzymes and are thought to be the active species for many difficult oxidation reactions effected by cytochrome P450 enzymes including hydroxylations of saturated C-H positions.[7] The one-electron reduced product of Compound I, a porphyrin-iron(IV)-oxo intermediate commonly called Compound II in reference to heme-containing enzymes, also acts as an

men@uic.edu.

Supporting Information Available. UV-visible spectra of **1b**, **1c**, **2b**, and **2c**, plots of rate constants for 1-phenylethanol oxidations, and dual parameter plots for oxidation reactions with **2a** and **2c**. This material is available free of charge via the Internet at http://pubs.acs.org.

oxidant of reactive species such as ascorbate, which is oxidized in a one-electron transfer oxidation reaction.[2,3]

Although Compound I and Compound II species in peroxidase and catalase enzymes and porphyrin-iron(IV)-oxo models have been known for decades, the detailed mechanisms of porphyrin-iron(IV)-oxo reactions are elusive, especially for model compounds reacting in two-electron, oxo-transfer oxidation reactions. For example, electron-withdrawing substituents in the aromatic rings of tetra-aryl-substituted porphyrins are expected to activate an iron-oxo derivative,[8] in which case 5,10,15,20-*tetrakis*(pentafluorophenyl)porphyrin-iron(IV)-oxo, (TPFPP)Fe^{IV}(O), should be more reactive than 5,10,15,20-tetramesitylporphyrin-iron(IV)-oxo, (TMP)Fe^{IV}(O). The oxidation potentials for (TPFPP)Fe^{IV}(O) and (TMP)Fe^{IV}(O) are in agreement with predictions based on the electron-withdrawing effects of the aryl substituents,[9,10] but the reactivities of the iron(IV)-oxo species as oxidants are not. (TPFPP)Fe^{IV}(O) epoxidizes alkenes slowly,[11] but (TMP)Fe^{IV}(O) apparently reacts 1–2 orders of magnitude more rapidly with styrene.[12] Moreover, in polar solvents, (TMP)Fe^{IV}(O) appeared to react by a disproportionation pathway to give a reactive species in the formal oxidation state of iron(V).[12] The apparent inverted reactivity pattern for porphyrin-iron(IV)-oxo species and possible disproportionation mechanisms for their reactions are reminiscent of oxidations by porphyrin-manganese(IV)-oxo species[13,14] and porphyrin-chromium(IV)-oxo species[15] that display similar kinetic behavior and/or disproportionate to give reactive porphyrin-metal(V)-oxo species.

Much of the mechanistic uncertainty regarding porphyrin-metal-oxo species is due to limited kinetic studies of these species.[6,16] Our group previously reported kinetics of reactions of high-valent porphyrin-metal-oxo species[14,17–19] and a heme-thiolate enzyme Compound I derivative[20] with several organic reductants to establish a catalogue of reactivities of these species for mechanistic analyses. In this work, we report rate constants for reactions of three porphyrin-iron(IV)-oxo complexes with alkenes and alcohols in acetonitrile solvent. Inverted reactivity patterns were found, with the porphyrin-iron(IV)-oxo species that would be predicted to be most reactive on the basis of electronic effects being the least reactive. The reaction mechanisms appear to involve predominantly disproportionation reactions that give iron(III) species and active oxidants that are assumed to be iron(IV)-oxo porphyrin radical cations.

Experimental Section

Materials

Free ligands 5,10,15,20-*tetrakis*(2,6-dichlorophenyl)porphyrin (TDCPP)H_2, 5,10,15,20-*tetrakis*(2,6-difluorophenyl)porphyrin (TDFPP)H_2, and 5,10,15,20-*tetrakis*(pentafluorophenyl)porphyrin (TPFPP)H_2 were purchased from FrontierSci Inc. and used as supplied. Iron(III) hydroxy complexes (TDCPP)Fe^{III}(OH) (**1a**), (TDFPP)Fe^{III}(OH) (**1b**), and (TPFPP)Fe^{III}(OH) (**1c**) were prepared by literature methods.[21–23] Commercial HPLC grade acetonitrile (99.9%) was distilled from P_2O_5 prior to use. Commercial *m*-chloroperoxybenzoic acid (MCPBA) (77%) was purified by crystallization from CH_2Cl_2 and dried *in vacuo*. All reactive substrates for kinetic studies were commercial materials of the highest available purity and were passed through a column of dry, active alumina (Grade I) before use.

Instrumentation

UV-visible spectra were recorded on an Agilent 8453 diode-array spectrophotometer, which was equipped with an Applied Photophysics RX2000 rapid mixing accessory for studying

fast reactions. ^{1}H NMR spectra were recorded on a 500 MHz instrument; chemical shifts are reported in ppm relative to internal TMS. EPR spectra were obtained at 77 K.

Preparation of porphyrin-iron(IV)-oxo derivatives 2

Ferric porphyrin hydroxyl complexes **1** were used as the precursors of **2**. When 2–4 equivalents of MCPBA was added to an acetonitrile solution of **1** (20 μM), the solution changed color from light red to dark red. The Soret bands were red-shifted in all cases, and the Q-bands indicated a change from ferric hydroxides to ferryl-oxo complexes **2**. UV-visible spectral details are listed in Table 1. In dilute solutions, complexes **2** were stable for hours at ambient temperature ($k_{obs} < 1 \times 10^{-4}$ s^{-1}). Higher concentration solutions were used for ^{1}H NMR spectra (5 mM), and the pyrrole proton chemical shifts are listed in Table 1. The more concentrated NMR samples were less stable than the dilute solutions used for UV-visible spectroscopy. The NMR samples were prepared at and spectra were recorded at ca. −40 °C, and, when these samples were warmed to room temperature, the solutions quickly changed color to green/brown. Upon subsequent cooling to ca. −35 °C, the ^{1}H NMR spectrum indicated formation of ferric high-spin complexes ($\delta_{pyrrole} > 100$ ppm).

Kinetic studies of reactions of porphyrin-iron(IV)-oxo species 2 with organic substrates

In a typical reaction, solutions of **2** (20 μM in CH_3CN) and an organic substrate with the desired concentration in CH_3CN were loaded into two gas-tight syringes. The samples were mixed in a UV-visible flow cell, and data was collected with delay times as short as 0.3 s. The decay rates for **2** and the formation rates for the ferric porphyrin products were measured at λ_{max} of the Q-band signals. The decay and growth traces were fit to single exponential solutions, and second-order rate constants were obtained from the pseudo-first-order rate constants via Equation 1 in the text.

Single turnover product studies

Solutions of the **2a** (20 μM) in CH_3CN were prepared as above. To these were added either benzyl alcohol or styrene such that the final substrate concentration was 0.10 M. The mixtures were stirred for 1–2 h. The samples were filtered through an alumina column to remove the porphyrin complex and analyzed by GC. Benzaldehyde and styrene oxide were identified by GC co-injection with authentic samples. The yields of products were determined relative to substrate using predetermined response factors. Control reactions using MCPBA in the absence of porphyrin complex **1a** gave only traces (<3% based on oxidant) of the oxidation products.

Results and Discussion

The systems studied are shown in Scheme 1. The commercial porphyrin ligands 5,10,15,20-*tetrakis*(2,6-dichlorophenyl)porphyrin, $(TDCPP)H_2$, 5,10,15,20-*tetrakis*(2,6-diflurophenyl)porphyrin, $(TDFPP)H_2$, and 5,10,15,20-*tetrakis*(pentaflurophenyl)porphyrin, $(TPFPP)H_2$ were converted to the iron(III) hydroxide complexes $(porph)Fe^{III}(OH)$ (**1**) by literature methods.[21–23] We employed hydroxide complexes in this work so that ligand exchange reactions with water would not result in new species and because the hydroxide complexes are easier to oxidize than the corresponding chloride complexes.

Oxidation of complexes **1** with purified MCPBA in acetonitrile gave the iron(IV)-oxo complexes **2** as indicated qualitatively by a color change from light red to deep red. In the UV-vis spectra of complexes **2**, the Soret bands were red-shifted from those of **1**, and the Q-bands were distinct. Figure 1A shows the time-resolved spectrum of **1a** as it is oxidized to **2a**, which is typical. Spectra of **1b**, **2b**, **1c**, and **2c** are in the Supporting Information. The hydroxide complex **1a** was fully oxidized to species **2a** with approximately 2 equivalents of

MCPBA at the concentrations used in UV-visible spectroscopic studies, but complexes **2b** and **2c** required approximately 4 equivalents of MCPBA. For solutions that were 10 μM in iron species in acetonitrile solvent, the approximate half-lives for formation of **2** from reactions of **1** were 1–10 s.

It is important to note that excess MCPBA was employed to oxidize the ferric complexes **1** to iron(IV)-oxo species **2**, but no excess MCPBA remained in the solutions containing species **2**. Thus, the kinetics of reactions of MCPBA are not convoluted into any of our kinetic values reported below. The absence of MCPBA in solutions of **2** was apparent from the kinetic studies where clean exponential behavior was observed with no lag time at the beginning of the reactions (e.g. Figure 1B). If excess MCPBA remained, a lag in the exponential decay and growth curves would be observed during the period when the excess MCPBA was being consumed. For example, the formation of **2a** in the reaction shown in Figure 1A had a half-life of ca. 30 s, whereas the reaction of **2a** with styrene shown in Figure 1B had a half-life of ca. 150 s. Because oxidation of **1a** to **2a** was faster than reaction of **2a** with substrate under these conditions, the presence of excess MCPBA in the reaction medium would result in a flat signal at the outset of the reaction of **2a**, which would continue until the excess MCPBA was depleted.

In balanced oxidation reactions of complexes **1** to give iron(IV)-oxo complexes **2,** only 0.5 equivalents of MCPBA should be required, but reactions of the porphyrin-iron(III) species with 0.5 or even 1 equivalent of MCPBA did not convert the iron(III) complex completely to the iron(IV)-oxo derivative. Our reactions required 2–4 equivalents of MCPBA to complete the oxidations; previously, Nam *et al.* reported that 4 equivalents of MCPBA were required for complete conversion of (TPFPP)Fe^{III}Cl to the oxo complex **2c**.[11] The excess MCPBA apparently is consumed when highly reactive iron-oxo transients react with the solvent, presumably forming formaldehyde cyanohydrin. Species **2** are the relatively unreactive sinks. In any event, once prepared, dilute solutions of porphyrin-iron(IV)-oxo species **2** in acetonitrile were stable for hours.

The production of porphyrin-iron(IV)-oxo species **2** instead of more highly oxidized iron(IV)-oxo porphyrin radical cations under the reaction conditions we used is noteworthy. In the present study with acetonitrile solvent, species **2** are formed, but MCPBA oxidations of porphyrin-iron(III) species in acetonitrile--water mixtures give the more highly oxidized species.[18] The origin of the water-stabilizing effect is not understood at the molecular level, but a similar phenomenon is known for porphyrin-manganese-oxo species.[14]

Our studies do not address directly the mechanisms of formation of species **2**. We assume that two-electron oxidations with oxo-transfer from MCPBA to species **1** give transients with a formal oxidation state of +5 on iron, and these species react with solvent in competition with comproportionation reactions with another molecule of **1** to give two molecules of iron(IV)-oxo species **2**. Such a pathway provides rationalizations for the excess MCPBA required to drive the reaction to completion and the formation of more highly oxidized iron-oxo species in acetonitrile-water mixtures. Alternatively, homolytic cleavage of an iron(III)-acyl peroxide complex can give an iron(IV)-oxo species directly.[24]

The iron(IV)-oxo species **2** were characterized by UV-visible, EPR, and NMR spectroscopies. The UV-visible spectrum of each species **2** (Figure 1 and Supporting Information) displayed a Soret band that was sharper, more intense, and red-shifted from that of the corresponding iron(III) species **1**. The Q-bands of the iron(IV)-oxo species **2** were distinct from those of the iron(III) species, and no peaks were observed at ca. 650 nm, the region at which the Q-bands of iron(IV)-oxo porphyrin radical cations absorb. In EPR studies, complexes **2** were silent, as expected for an iron(IV) species ($S = 1$).

^{1}H NMR spectra of complexes **1** and **2** in CD_3CN solutions showed broad peaks for the macrocycle pyrrole protons that were highly characteristic with absorbances at ca. 105 ppm for the iron(III) complexes **1** and ca. 5 ppm for the iron(IV)-oxo species **2**. The large shift for the pyrrole protons in species **1** ($\delta > 100$ ppm) is consistent with high-spin ferric complexes. The chemical shifts of the pyrrole protons in iron(IV)-oxo complexes **2** suggest six-coordinate iron species;[25] we assume that the sixth coordination site is occupied by acetonitrile. Some of the spectral properties of species **1** and iron(IV)-oxo species **2** are listed in Table 1. For comparison, the spectral properties of the well-studied analogous iron-tetramesitylporphyrin (TMP) complexes[12,22,25] also are listed.

Figure 2A shows the NMR spectrum of **2c**, which is the cleanest NMR spectrum we obtained; the signals for MCPBA and *m*-chlorobenzoic acid, which overlap, were observed in the absence of the iron species. A Curie plot for the pyrrole protons in **2c** (Figure 2B) is similar to those for other iron(IV) species and confirms the paramagnetic character of **2c**.[25,26]

Differences in stabilities of high concentration samples (ca. 5 mM for NMR studies) and low concentration samples (ca. 20 μM for UV-vis spectra) have been noted before.[27] High conversions of **1** to **2** at the concentrations needed for NMR spectra required a large excess of MCPBA, and low reaction temperatures (ca. −35 °C). Even with those conditions, the formation of **2a** and **2b** was not complete, although new signals for the pyrrole protons of **2** could be detected. In contrast, the dilute samples of **2** in CH_3CN used for UV-visible spectroscopy were prepared at room temperature and were stable for hours. In the discussion below, we reason that the iron(IV)-oxo derivatives **2** disproportionate and that the active oxidant in the systems studied here are actually iron(IV)-oxo porphyrin radical cations. In such a case, concentration dependent decay of species **2** would be observed when the disproportionation reactions were fully or partially rate limiting, but accelerated decay is not required if the disproportionation--comproportionation reactions are fast relative to the oxidations. We speculate that the accelerated decay of species **2** in the high concentration NMR samples reflects increased velocities for oxidations of the porphyrin macrocycles in competition with oxidation of solvent molecules, which must be concentration dependent.

The primary objective of this work was kinetic studies of the reactions of the iron(IV)-oxo species. At low concentrations used in UV-visible spectroscopy studies, species **2** were relatively stable. For example, the rate constant for first-order decay of a 10 μM solution of **2a** used for UV-visible spectroscopy was $k \approx 1 \times 10^{-4}$ s^{-1}. Qualitatively, the order of reactivity for decay in CH_3CN solutions was **2a** > **2b** > **2c**, which presages the inverted reactivity order observed with organic reductants.

We studied reactions of iron-oxo complexes **2** with alkenes and with alcohols using UV-visible spectroscopy with low concentrations of iron species. Under turnover conditions with porphyrin-iron(III) species as catalysts and MCPBA or other sacrificial oxidants, epoxides and carbonyl compounds, respectively, are the major products formed from these substrates.[6] We performed cursory product studies for the apparent "stoichiometric" reactions of the iron(IV)-oxo species **2a**. Thus, solutions of **2a** (20 μM) in CH_3CN were allowed to react with 5000-fold excesses of benzyl alcohol and styrene, and the reaction mixtures were analyzed by GC. Under these single turnover conditions, the major product formed from benzyl alcohol was benzaldehyde (70%), and the major product formed from styrene was styrene oxide (60%), where the yields were calculated based on a stoichiometry of 2 equivalents of **2a** reacting with one equivalent of the organic substrate.

Kinetic studies employed large excesses of substrates so that all decay reactions of iron(IV)-oxo species were pseudo-first-order. The results in Figure 1B and Figure 3A are typical. The

time-resolved spectrum in Figure 1B shows clean conversion of iron(IV)-oxo **2a** to **1a** as it reacts with styrene, and the isosbestic points observed at 442, 529, and 567 nm indicate that no other porphyrin-iron intermediate accumulated to detectable levels during the reaction. We specifically note that the iron-containing products were hydroxide complexes **1** and not the porphyrin-iron(III) *m*-chlorobenzoate complexes, which have distinct UV-visible spectra.[28] Furthermore, the UV-visible spectra of the products excluded iron(II) species.[29]

Figure 3A shows kinetic traces at 418 nm for reactions of **2a** with different concentrations of styrene. The traces were well fit to single exponential decay, as expected for reactions under pseudo-first-order conditions. The results were analyzed with Equation 1, where k_{obs} is the observed rate constant, k_0 is a background rate constant for decay, k_{ox} is the second-order rate constant for reaction of the iron(IV)-oxo species with substrate, and [Sub] is the concentration of substrate. The inset in Figure 3A shows the plot according to Equation 1 where the slope of the line is the second-order rate constant k_{ox}. Figure 3B shows data for reactions of iron(IV)-oxo species **2** with diphenylmethanol, and Figure S3 in Supporting Information shows data for reactions with 1-phenylethanol. Apparent second-order rate constants for reactions of iron(IV)-oxo species **2** with several substrates are listed in Table 2. With little exception, the apparent order of reactivity of the iron-oxo species with a given substrate was **2a** > **2b** > **2c**.

$$k_{obs}=k_0+k_{ox}[\mathrm{Sub}] \quad (1)$$

Under the conditions we employed, concentrations of substrates were thousands of times as large as those of the oxo complexes. Therefore, the concentration of product formed in the initial substrate oxidation was much smaller than the concentration of substrate, and secondary oxidations were not an issue. The single exponential data fits confirm that the initial oxidation reactions were the major reaction pathways. If secondary oxidations were important, the decay traces would not show pseudo-first-order behavior, and plots of k_{obs} solved for pseudo-first-order conditions against concentrations of substrate would not be linear.

The observed reactivity order in regard to the porphyrin-iron-oxo species is not consistent with predictions based on the electron-withdrawing effects of the aryl groups of the porphyrin macrocycles. The redox potentials for oxidations of porphyrin-iron(III) complexes show that the electron demand of the macrocycles is in the order **2a** < **2b** < **2c**.[9,10] Increasing electron demand from the macrocycle should result in increasingly reactive metal-oxo complexes,[8] and that order of reactivity was found for iron(IV)-oxo porphyrin radical cations.[18,30] With complexes **2**, however, the opposite kinetic trend is found.

One logical explanation for the observed relative reactivities of complexes **2** is that species **2** are not the predominant oxidants in the reactions. If the porphyrin-iron(IV)-oxo intermediates rapidly establish a disproportionation equilibrium, then the major oxidant in the system might be the high-valent iron-oxo species (**3**) with a formal oxidation state of iron(V), presumably an iron(IV)-oxo porphyrin radical cation (Scheme 2). Such an equilibrium with reaction of a high-valent iron-oxo species is consistent with reactions of (TMP)Fe^{IV}(O) in polar solvents.[13] Similarly, porphyrin-manganese(IV)-oxo species appear to react largely or entirely via porphyrin-manganese(V)-oxo species produced in a disproportionation equilibrium the same as that shown in Scheme 2.[14]

Oxidation reactions proceeding according to the mechanism in Scheme 2 are consistent with the findings of apparent inverted reactivity patterns. The disproportionation equilibrium will be increasingly less favorable as the electron demand of the macrocycle increases. Thus, for

example, smaller concentrations of active oxidant **3c** are expected for the (TPFPP) system **2c** than for the other iron(IV)-oxo species, resulting in slower consumption of species **2c**. That is, the changes in electron demand of the macrocycle can have counteracting effects on the observed rates of reactions; reactions of the true oxidants increase in rate with increasing electron withdrawl by the macrocycle, but the population of reactive species decreases with increasing electron demand of the macrocycle. Furthermore, oxidation by a species in a higher metal valence than species **2** also provides a convenient "two-electron" oxo transfer reagent that can react without the formation of intermediate organic radical ions. The Scheme also presents a reasonable explanation for how two-electron oxo-transfer oxidation reactions of porphyrin-metal(III) complexes by sacrificial oxidations such as MCPBA or PhIO ultimately lead to porphyrin-metal-oxo products with metals increased in oxidation state by only +1.

One test of the disproportionation equilibrium in Scheme 2 is to attempt to suppress the oxidation reaction by adding excess complex **1** to the reaction mixture. A series of reactions of **2a** with benzyl alcohol was performed with varying amounts of iron(III) species **1a** added and other concentrations held constant. The reaction rate clearly decreased as increasing amounts of **1a** were added. For the reaction sequence for Scheme 2 with a fast equilibrium relative to the substrate oxidation, the rate law for oxidation would be given by Equations 2 and 3, where $k_{\mathbf{3}}$ is the second-order rate constant for oxidation by species **3**, and K_{eq} is the equilibrium constant for the disproportionation reaction. Under pseudo-first-order conditions, the observed rate constant k_{obs} is expected to be inversely proportional to the concentration of species **1**. Figure 4 shows the results of the kinetic studies with added **1a** in log-log format. As predicted from Scheme 2 and Eq 3, the kinetic order for **1a** is approximately −1.

$$d[\text{Product}]/dt = k_{\mathbf{3}}[\text{Sub}][\mathbf{3}] \quad (2)$$

$$d[\text{Product}]/dt = k_{\mathbf{3}}K_{eq}[\text{Sub}][\text{H}_2\text{O}][\mathbf{2}]^2/[\mathbf{1}] \quad (3)$$

Another test of the mechanism in Scheme 2 is possible in principle but not in practice. Addition of water to the reaction mixture might be expected to push the equilibrium in Scheme 2 to the right and increase the overall rate of reaction by increasing the concentration of active oxidant **3**. When transient **2a** was produced in acetonitrile--water with an excess of MCPBA, formation of species **3a** was observed by UV-visible spectroscopy. In fact, it was possible to convert **2a** completely to the iron(IV)-oxo porphyrin radical cation **3a** with excess MCPBA. Unfortunately, water is known to stabilize iron(IV)-oxo porphyrin radical cations,[18,27] which explains why species **3a** accumulated in the acetonitrile--water mixture, and kinetic studies with water present cannot be compared directly to those in the absence of water. The stabilization of the Compound I analogue **3a** by water is similar to stabilization previously observed with water-soluble porphyrin-iron-oxo species[27] and porphyrin-manganese(V)-oxo species.[14] The origin of the stabilizing effect is not obvious[6] and deserves further study, but the point for this work is that we could not use the results of reactions in acetonitrile--water to understand the equilibrium in Scheme 2.

The important conclusion from the above studies is that when reactions of iron(IV)-oxo species are studied, the active oxidants apparently were iron-oxo derivatives in higher oxidation states than the observable species **2**. This complicates an analysis of the kinetic

data in regard to the absolute values for the observed rate constants because the experimental values are most likely the products of the disproportionation equilibrium constants times the rate constants for oxidations by the (undetectable) high oxidation state metal-oxo species or also could be convolutions of rate constants for these two processes if the equilibrations are not fast relative to the oxidations. Nonetheless, relative rate constants for reactions by a given species **2** can be analyzed in a meaningful manner if the equilibria in Scheme 2 are rapidly established relative to the oxidation reactions proper. In considerations of relative rate constants, the concentration of the high valent iron-oxo species would cancel in the relative rate expression, and the relative rate constants for reactions of the high valent iron-oxo species **3** would be evaluated directly.

In the analysis that follows, we assume that the equilibria in Scheme 2 are rapidly established for the three iron(IV)-oxo species. Thus, the rate constants for disproportionation and comproportionation are expected not to be convoluted with the relative rate constants for oxidation reactions by the high-valent iron-oxo species **3**. This premise is supported by the excellent free energy correlations found for reactions of the series of substituted benzyl alcohols, where the velocities of the reactions varied by more than 2 orders of magnitude for reactions of benzyl alcohol and 4-methoxybenzyl alcohol.

The most electron-deficient porphyrin we used was the *tetrakis*(pentafluorophenyl)-substituted system, (TPFPP), in **1c**. Rate constants for reactions of the Compound I analogue $(TPFPP)^{+\bullet}Fe^{IV}(O)(ClO_4)$ in CH_2Cl_2 with *cis*-cyclooctene, cyclohexene, and *cis*-stilbene are 120, 220, and 190 M^{-1} s^{-1},[18] or about 4 orders of magnitude larger than the rate constants found here for reactions of **2c** with the same substrates. These ratios provide a crude approximation for the equilibrium constant in Scheme 2, although it is possible that the difference in solvents for the two sets of studies might have a large effect on the equilibria. The equilibrium constant deduced for the analogous porphyrin-manganese(IV)-oxo species, $(TPFPP)Mn^{IV}(O)$, disproportionating to the manganese(III) species and manganese(V)-oxo species in CH_3CN solvent was of the same order of magnitude.[14]

The rate constants for the alcohol oxidations demonstrate both electronic and steric effects. Rate constants for reactions of 1-phenylethanol were larger than those for reactions of benzyl alcohol, apparently reflecting electronic effects that result in a weaker benzylic C-H bond in the former alcohol. Diphenylmethanol, which has a much reduced C-H bond energy from that in benzyl alcohol,[31] reacted less rapidly than 1-phenylethanol, however, and one concludes that steric effects were important in this case with limited access of the bulky alcohol to the iron-oxo species. The kinetic isotope effects in oxidations of benzyl alcohol and its perdeuterated analogue were k_H/k_D = 5.2, 4.5, and 5.7 for **3a**, **3b**, and **3c**, respectively, indicating a large degree of C-H bond breaking in the transition states for the reactions. Similar kinetic isotope effects were observed in hydroxylations of benzyl alcohol by other transition metal-oxo complexes.[32,33]

The oxidations of the *para*-substituted benzyl alcohols provide insights into the electronic demands in the transition states of the oxidation reactions. A conventional Hammett function analysis with the σ substituent values gives poor results, and analysis with σ^+ substituent values leads to some improvement (Figure 5A). Analysis of the rate constants with a dual parameter function that separates polar and spin delocalization effects of the substituents gives excellent fits, however, and appears to be most appropriate for these reactions. We used the dual parameter analysis developed by Jiang.[34] In this approach, *para*-substituents have a polar substituent value, σ_{mb} in Equation 4, and a spin-delocalization substituent value, $\sigma_{jj}^{\bullet}$. The relative rate constants for reactions are analyzed by iteration of the ρ values to give the best fit for the line.[34] Figure 5B shows the dual parameter fit for reactions of **2b**, where the correlation coefficient is R = 0.999. Good fits also were obtained for **2a** (R =

0.995) and **2c** (R = 0.994) (Supporting Information). The results for the dual parameter analysis are listed in Table 3, which also contains the ρ^+ values that were found when the data was analyzed in terms of the Hammett σ^+ substituent values.

$$\log(k_Y/k_H)=\rho_{mb}\sigma_{mb}+\rho_{jj}^{\bullet}\sigma_{jj}^{\bullet}+C \quad (4)$$

As expected for electrophilic oxidants, the ρ^+ values are negative, demonstrating positive charge development on the substrate in the transition states for the oxidation reactions. In the dual parameter approach, ρ_{mb} also is negative for the same reason. The ρ_{mb} values and ρ^+ values are similar for the three oxidants, which is the expected behavior because charge development in reactions of porphyrin-metal-oxo species is sensitive to the axial ligand but relatively insensitive to the aryl group substituents of the porphyrin. The degree of charge development found here is similar to that reported previously (ρ^+ values in the range of −1.8 to −2.0) for styrene epoxidation reactions effected by iron(IV)-oxo porphyrin radical cations with the weak- and intermediate-binding axial ligands hydroxide,[35] triflate,[36] and perchlorate.[18]

The spin delocalization reaction parameters $\rho_{jj}^{\bullet}$ obtained in the dual parameter analyses are instructive. These values decrease as the porphyrin radical stabilizing effects increase, reflecting reduced radical character developing on the substrate with a more stabilizing porphyrin. The absolute values of the $\rho_{jj}^{\bullet}$ terms are larger than those of the polar reaction parameters ρ_{mb}, with $\rho_{mb}/\rho_{jj}^{\bullet}$ in the range of −0.7 to −0.9. Such ratios demonstrate that both polar and spin delocalization effects are important in the benzyl alcohol oxidation reactions, [34] and the values of the ratios obtained here are similar to those found for some additions of electrophilic radicals to substituted styrenes[37,38] and for benzylic H-atom abstractions from substituted toluenes by the electrophilic bromine atom.[39] Development of radical character at the benzylic position in the transition states for oxidations of the benzyl alcohols is likely the major reason why the kinetic results did not correlate well with conventional Hammett σ and σ^+ values.

In summary, the studies reported in this work add kinetic results for transition metal-oxo reactions that can be compared with other kinetic data to understand mechanistic details of oxidation reactions. Inverted reactivity patterns were found, with the iron(IV)-oxo species containing the most electron-withdrawing porphyrin reacting least rapidly, similar to earlier findings with porphyrin-manganese(IV)-oxo species,[14] and the rate of the oxidation reaction was shown to be inversely proportional to the concentration of added porphyrin-iron(III) complex. These results indicate that porphyrin-iron(IV)-oxo species disproportionate to give iron(III) species and high-valent iron-oxo species, presumed to be iron(IV)-oxo porphyrin radical cations, that are the true oxidants in reactions with alkenes and alcohols. Linear free energy analyses of reactions of *para*-substituted benzyl alcohols indicate that considerable amounts of positive charge and spin character develop on the benzylic carbons in the transition states for the oxidation reactions.

Supplementary Material

Refer to Web version on PubMed Central for supplementary material.

Acknowledgments

We thank the National Institutes of Health and the National Science Foundation for financial support and Prof. R. Zhang for helpful discussions.

References

1. Ortiz de Montellano, PR., editor. Cytochrome P450 Structure, Mechanism, and Biochemistry. 3. Kluwer; New York: 2005.
2. Dawson JH. Science 1988;240:433–439. [PubMed: 3358128]
3. Sono M, Roach MP, Coulter ED, Dawson JH. Chem Rev 1996;96:2841–2887. [PubMed: 11848843]
4. Denisov IG, Makris TM, Sligar SG, Schlichting I. Chem Rev 2005;105:2253–2277. [PubMed: 15941214]
5. Sheldon, RA., editor. Metalloprophyrins In Catalytic Oxidations. Marcel Dekker; New York: 1994.
6. Meunier B. Chem Rev 1992;92:1411–1456.
7. Makris TM, von Koenig K, Schlichting I, Sligar SG. J Inorg Biochem 2006;100:507–518. [PubMed: 16510191]
8. Dolphin D, Traylor TG, Xie LY. Acc Chem Res 1997;30:251–259.
9. Lee WA, Calderwood TS, Bruice TC. Proc Natl Acad Sci USA 1985;82:4301–4305. [PubMed: 3859865]
10. Lim MH, Lee YJ, Goh YM, Nam W, Kim C. Bull Chem Soc Jpn 1999;72:707–713.
11. Nam W, Park SE, Lim IK, Lim MH, Hong JK, Kim J. J Am Chem Soc 2003;125:14674–14675. [PubMed: 14640620]
12. Groves JT, Gross Z, Stern MK. Inorg Chem 1994;33:5065–5072.
13. Groves JT, Stern MK. J Am Chem Soc 1988;110:8628–8638.
14. Zhang R, Horner JH, Newcomb M. J Am Chem Soc 2005;127:6573–6582. [PubMed: 15869278]
15. Groves JT, Kruper WJ Jr, Haushalter RC, Butler WM. Inorg Chem 1982;21:1363–1368.
16. Nam W. Acc Chem Res 2007;40:0000–0000.
17. Zhang R, Newcomb M. J Am Chem Soc 2003;125:12418–12419. [PubMed: 14531679]
18. Pan Z, Zhang R, Newcomb M. J Inorg Biochem 2006;100:524–532. [PubMed: 16500709]
19. Pan Z, Zhang R, Fung LWM, Newcomb M. Inorg Chem 2007;46:1517–1519. [PubMed: 17284026]
20. Zhang R, Nagraj N, Lansakara-P DSP, Hager LP, Newcomb M. Org Lett 2006;8:2731–2734. [PubMed: 16774243]
21. Adler AD, Longo FR, Kampas F, Kim J. J Inorg Nucl Chem 1970;32:2443–2445.
22. Cheng RJ, Latos-Grazynski L, Balch AL. Inorg Chem 1982;21:2412–2418.
23. Woon TC, Shirazi A, Bruice TC. Inorg Chem 1986;25:3845–3846.
24. Yamaguchi K, Watanabe Y, Morishima I. J Am Chem Soc 1993;115:4058–4065.
25. Balch AL, Chan YW, Cheng RJ, La Mar GN, Latos-Grazynski L, Renner MW. J Am Chem Soc 1984;106:7779–7785.
26. Groves JT, Quinn R, McMurry TJ, Nakamura M, Lang G, Boso B. J Am Chem Soc 1985;107:354–360.
27. Bell SEJ, Cooke PR, Inchley P, Leanord DR, Lindsay Smith JR, Robbins A. J Chem Soc, Perkin Trans 2 1991:549–559.
28. Machii K, Watanabe Y, Morishima I. J Am Chem Soc 1995;117:6691–6697.
29. Ghiladi RA, Kretzer RM, Guzei I, Rheingold AL, Neuhold YM, Hatwell KR, Zuberbuhler AD, Karlin KD. Inorg Chem 2001;40:5754–5767. [PubMed: 11681882]
30. Fujii H. J Am Chem Soc 1993;115:4641–4648.
31. McMillen DF, Golden DM. Ann Rev Phys Chem 1982;33:493–532.
32. Zhang R, Yu WY, Lai TS, Che CM. Chem Commun 1999:1791–1792.
33. Oh NY, Suh Y, Park MJ, Seo MS, Kim J, Nam W. Angew Chem Int Ed 2005;44:4235–4239.
34. Jiang XK. Acc Chem Res 1997;30:283–289.
35. Groves JT, Watanabe Y. J Am Chem Soc 1986;108:507–508.
36. Song WJ, Ryu YO, Song R, Nam W. J Biol Inorg Chem 2005;10:294–304. [PubMed: 15827730]
37. Guo GHX, Sun SSX, Ji GZ, Jiang XK. J Chem Res S 1993:166–167.
38. Jiang XK, Liu WWZ, Wu SH. J Phys Org Chem 1994;7:96–104.

39. Jiang XK, Liu WWZ, Wu SH. Tetrahedron 1994;50:7503–7512.

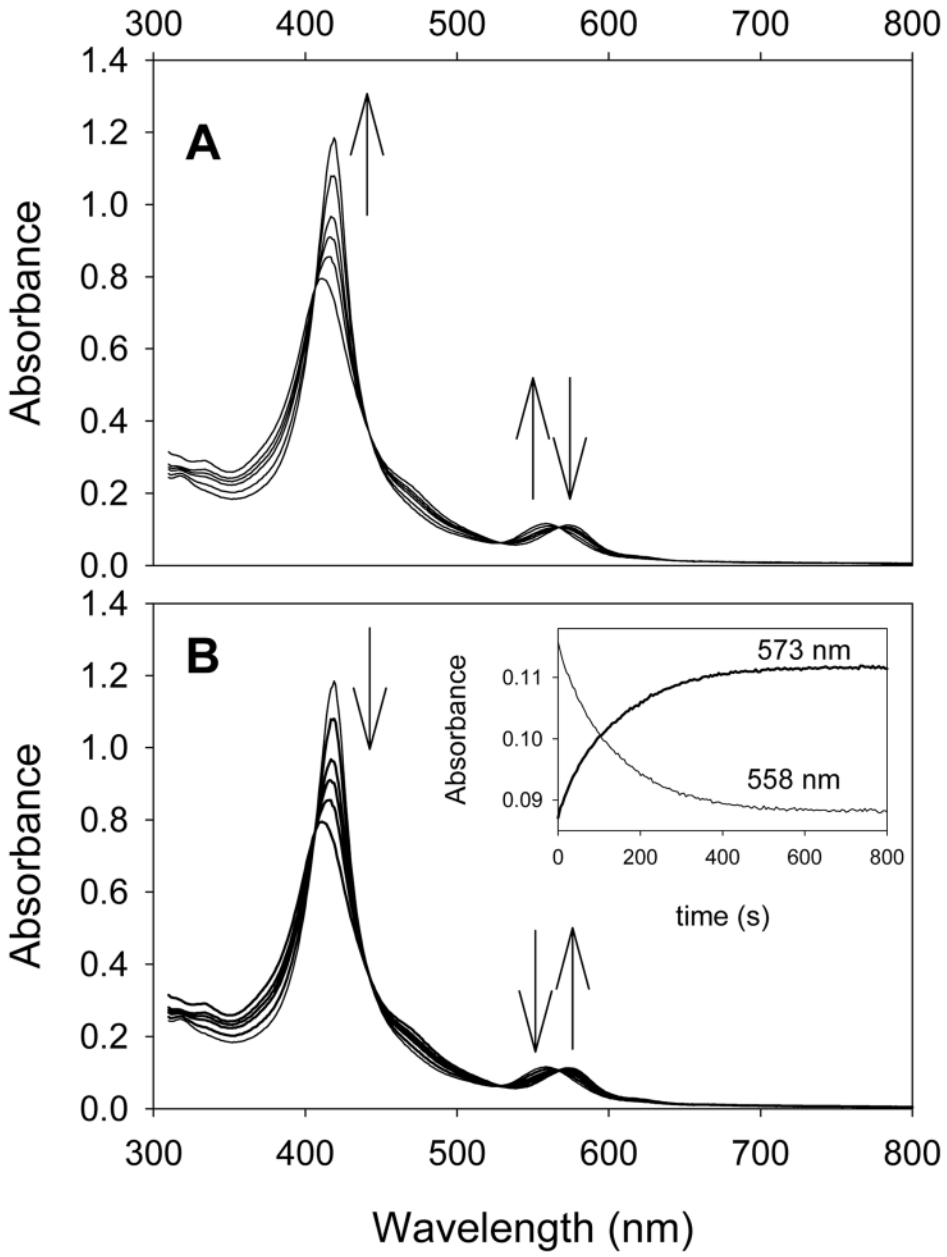

Figure 1.

(**A**) Time-resolved UV-visible spectrum for conversion of **1a** (10 μM) to **2a** in CH_3CN by reaction with 2 equivalents of MCPBA. The initial trace was recorded at 0.3 s after mixing, and subsequent traces were recorded at 8 s intervals. (**B**) Time-resolved spectrum for reaction of **2a** with 0.4 M styrene; the inset shows the kinetic traces at 558 and 573 nm.

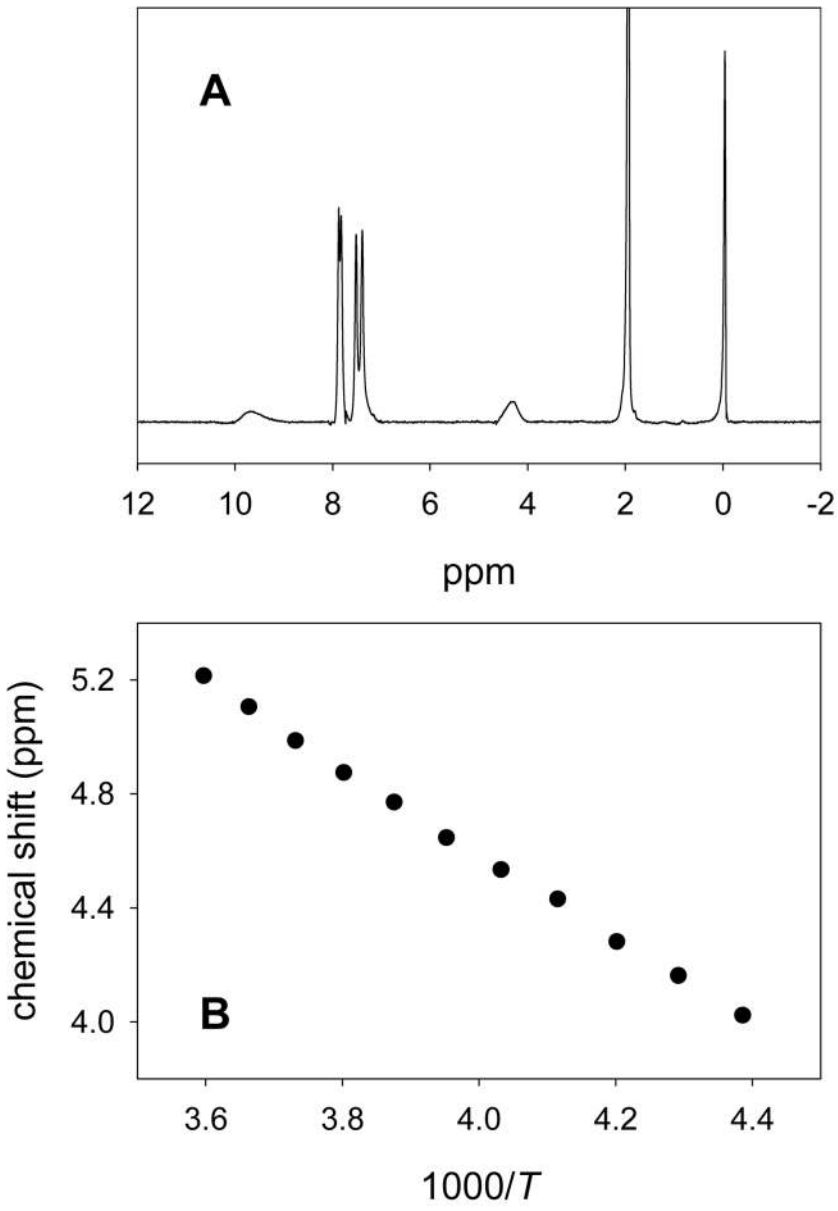

Figure 2.

(A) ^{1}H NMR spectrum of **2c** in CD_3CN at −35 °C. The pyrrole protons of **2c** absorb at δ 4.3. Other signals in the spectrum are from TMS (δ 0), CHD_2CN (δ 2), and *m*-chlorobenzoic acid and/or MCPBA (δ 7–8 and 9.5). (B) Curie plot for chemical shifts of the pyrrole protons in **2c** as a function of temperature between 5 and −45 °C.

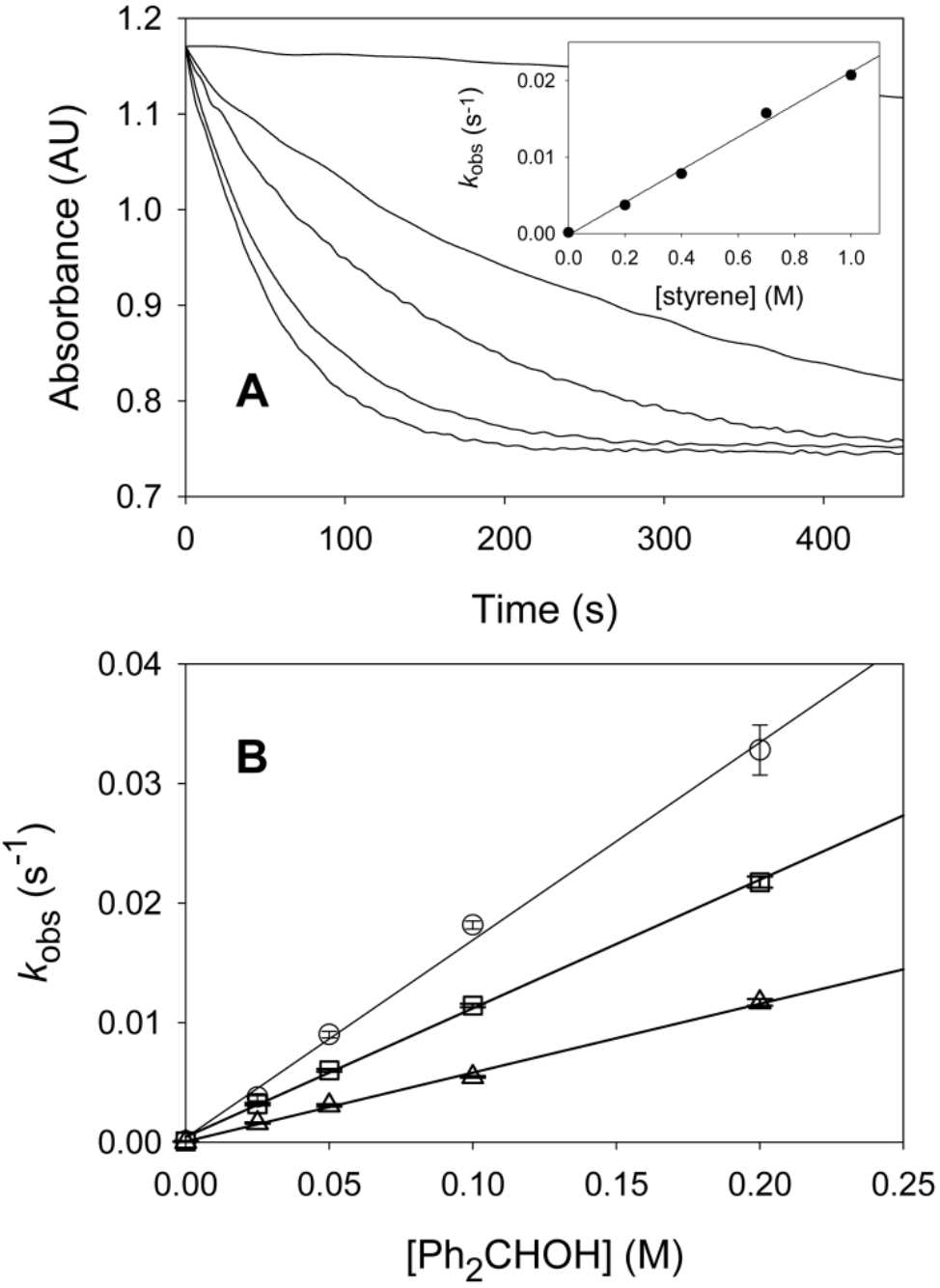

Figure 3.

Kinetic results. (**A**) Kinetic traces at 418 nm for reactions of iron(IV)-oxo species **2a** in CH_3CN with (from the top) 0.0, 0.2, 0.4, 0.7, and 1.0 M styrene. The inset shows a plot of the data according to Equation 1. (**B**) Observed rate constants for reactions of diphenylmethanol with **2a** (◦), **2b** (□), and **2c** (▵).

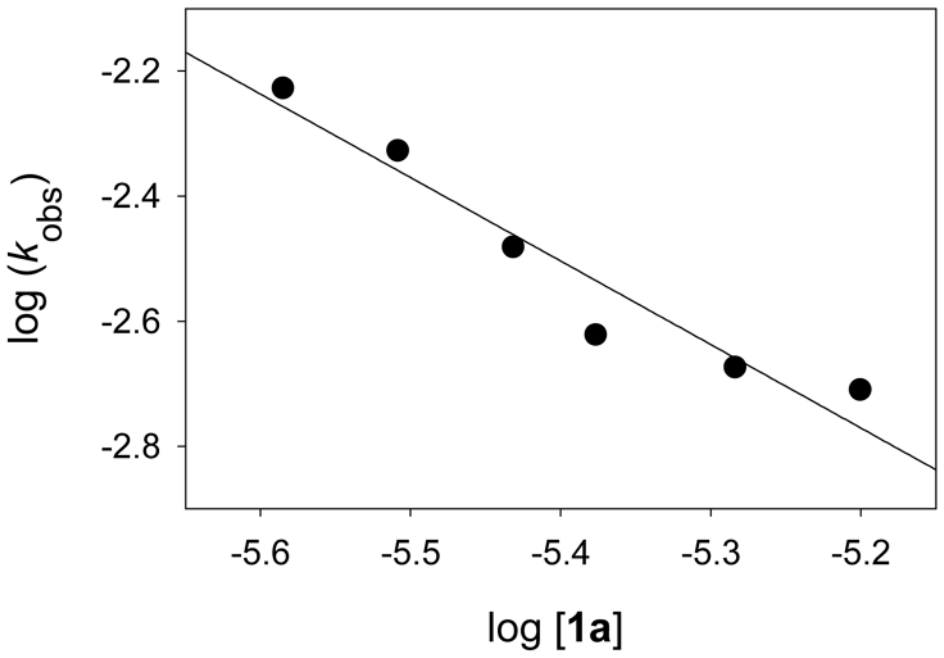

Figure 4.
Observed rate constants for reaction of benzyl alcohol with (TDCPP)Fe^{IV}(O) (**2a**) in the presence of added complex **1a**. The slope of the line is −1.34 ± 0.36.

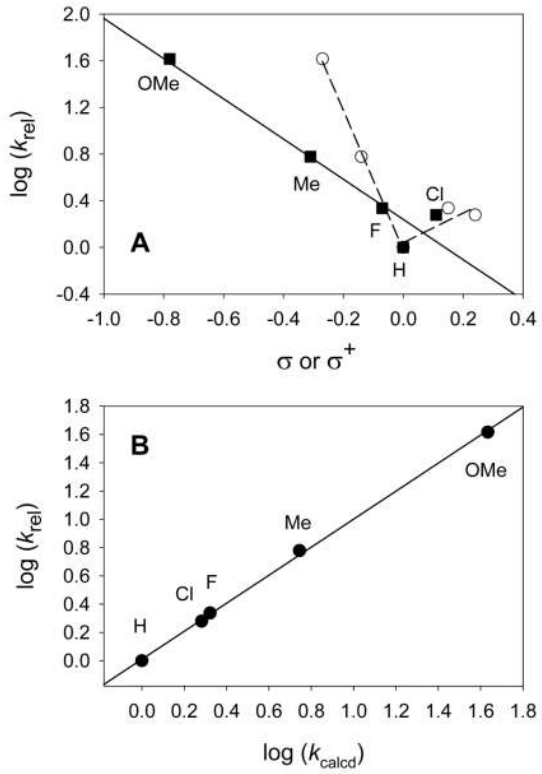

Figure 5.

Linear free energy relationships for rate constants for reactions of **2b** with benzyl alcohols, where the labels indicate the substituent on the benzyl alcohol. (**A**) Hammett plots with σ values (open circles and dashed lines) and σ^+ values (squares and solid line). (**B**) Dual parameter analysis after Jiang;[34] the calculated rate constants are for Equation 4 in the text using the ρ values for in Table 3.

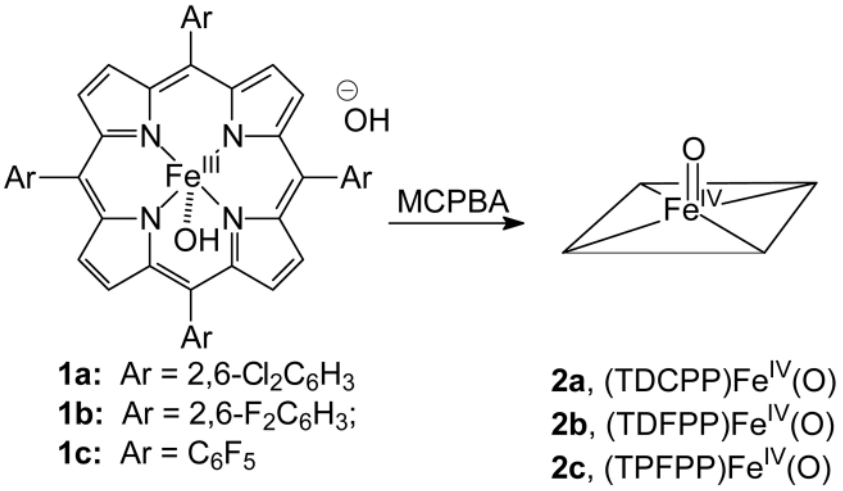

Scheme 1.

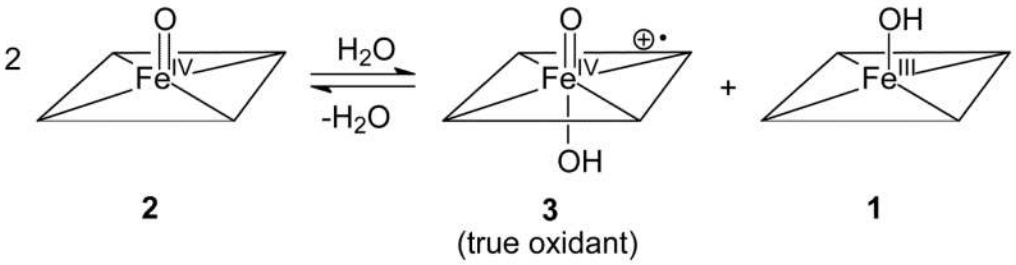

2 **3** (true oxidant) **1**

Scheme 2.

Table 1

Spectral Properties of Iron Species **1** and Iron(IV)-Oxo Complexes **2**.[a]

Porphyrin-Iron	Soret λ_{max} (nm)	Q-band λ_{max} (nm)	$\delta_{pyrrole}$ (ppm)[b]
1a, (TDCPP)Fe^{III}(OH)	412	573	105.8
1b, (TDFPP)Fe^{III}(OH)	405	567	104.0
1c, (TPFPP)Fe^{III}(OH)	402	564	105.2
(TMP)Fe^{III}(OH)[c]	418	580	116.4
2a, (TDCPP)Fe^{IV}(O)	418	558	5.9
2b, (TDFPP)Fe^{IV}(O)	412	551	4.1
2c, (TPFPP)Fe^{IV}(O)	411	547	4.3
(TMP)Fe^{IV}(O)[c]	418	540	8.4

[a] UV-visible spectra in CH_3CN at room temperature, and NMR spectra in CD_3CN at −35 °C unless noted.

[b] Chemical shift of pyrrole protons downfield from TMS.

[c] (TMP) = 5,10,15,20-*tetrakis*(2,4,6-trimethylphenyl)porphyrinato. UV-visible spectrum in CH_2Cl_2 from ref [12]. NMR spectrum in toluene-d_8 from ref [25].

Table 2

Apparent Second-Order Rate Constants for Reactions of Porphyrin-Iron(IV)-Oxo Species **2** in Acetonitrile.[a]

	$100 \times k_{ox}$ (M^{-1} s^{-1})		
Substrate	**(TDCPP)Fe^{IV}(O)**	**(TDFPP)Fe^{IV}(O)**	**(TPFPP)Fe^{IV}(O)**
1-phenylethanol	21.3 ± 1.8	12.7 ± 0.8	7.7 ± 1.1
diphenylmethanol	16.7 ± 1.1	10.8 ± 0.4	4.9 ± 0.2
benzyl alcohol	3.3 ± 0.2	3.0 ± 0.1	3.0 ± 0.1
benzyl alcohol-d_7	0.64 ± 0.08	0.66 ± 0.02	0.53 ± 0.01
4-chlorobenzyl alcohol	6.7 ± 0.2	5.7 ± 0.2	4.2 ± 0.2
4-fluorobenzyl alcohol	7.2 ± 0.3	6.5 ± 0.4	5.3 ± 0.3
4-methylbenzyl alcohol	28.0 ± 1.3	18.0 ± 1.3	17.1 ± 0.9
4-methoxybenzyl alcohol	168 ± 8	124 ± 4	90 ± 6
cis-cyclooctene	9.8 ± 0.2	nd[b]	1.8[c]
cyclohexene	7.3 ± 0.1	nd[b]	6.0[c]
cis-stilbene	4.2 ± 0.3	4.1 ± 0.1	2.1 ± 0.1
styrene	1.9 ± 0.1	1.6 ± 0.1	0.9 ± 0.1
4-methylstyrene	7.4 ± 0.4	5.1 ± 0.6	3.5 ± 0.1

[a] Apparent second-order rate constants for reactions at 22 ± 2 °C. The values are averages of 2 or 3 runs, and the stated errors are 2σ.

[b] Not determined.

[c] Rate constant estimated from results in ref [11].

Table 3

Reaction Parameters for Oxidations of Benzyl Alcohols.[a]

Porphyrin-Iron-Oxo	ρ^+	ρ_{mb}	$\rho_{jj}^{\bullet}$
2a, (TDCPP)Fe^{IV}(O)	−1.8	−1.58	2.34
2b, (TDFPP)Fe^{IV}(O)	−1.7	−1.51	2.04
2c, (TPFPP)Fe^{IV}(O)	−1.7	−1.46	1.61

[a] ρ^+ values are reaction parameters obtained by least-squares fit for data against Hammett σ^+ substituent values. ρ_{mb} and $\rho_{jj}^{\bullet}$ are values from least squares fits for the dual parameter equation developed by Jiang; with σ_{mb} and $\sigma_{jj}^{\bullet}$ values from ref [34].